Effective field theory of interacting π electrons

J. D. Barr, C. A. Stafford, and J. P. Bergfield

Phys. Rev. B **86**, 115403 — Published 4 September 2012

DOI: 10.1103/PhysRevB.86.115403

Effective Field Theory of Interacting π-Electrons

J. D. Barr* and C. A. Stafford
Department of Physics, University of Arizona, 1118 East Fourth Street, Tucson, AZ 85721

J. P. Bergfield
Nano-Science Center and Department of Chemistry, University of Copenhagen, Universitetsparken 5, 2100 Copenhagen Ø, Denmark

We develop a π-electron effective field theory (π-EFT) wherein the two-body Hamiltonian for a π-electron system is expressed in terms of three effective parameters: the π-orbital quadrupole moment, the on-site repulsion, and a dielectric constant. As a first application of this π-EFT, we develop a model of screening in molecular junctions based on image multipole moments, and use this to investigate the reduction of the HOMO-LUMO gap of benzene. Beyond this, we also use π-EFT to calculate the differential conductance spectrum of the prototypical benzenedithiol-Au single-molecule junction and the π-electron contribution to the van der Waals interaction between benzene and a metallic electrode.

I. INTRODUCTION

Owing to the profound versatility of the carbon-carbon bond, organic molecules form the basis for a myriad of potential nanotechnology applications. Many of these make use of the ability of conjugated organic molecules to conduct electricity, in which case the system of delocalized π-electrons plays a role analogous to that of the conduction band in a conventional semiconductor. In such devices, the most important degrees of freedom from a technological perspective are those associated with these current-carrying π-electrons.

The main motivation of the present work is to derive a model Hamiltonian for π-electron systems to facilitate the study of many-body effects on transport through molecular heterojunctions. The standard paradigm for molecular junction transport calculations involves local or semilocal approximations to density functional theory (DFT) combined with nonequilibrium Green's functions (NEGF). This DFT-NEGF approach[1] has tremendous advantages in terms of computational efficiency and chemical realism. However, it has notorious difficulties describing the energetics most relevant for electron transport, namely the energy level alignment between molecule and metal electrodes, and the fundamental (or HOMO-LUMO) gap. Some possible underlying reasons for this are (i) the failure to include nonlocal correlations responsible for screening of intramolecular interactions by nearby metal electrodes;[2,3] (ii) self-interaction error;[4–7] and (iii) omission of the derivative discontinuity[8,9] needed to describe the quantization of the molecular charge within the junction.[10] Self-consistent many-body perturbation theory[11] is able to overcome hurdles (i) and (ii), but still leaves (iii) as an open problem.

An alternative approach is to formulate a model including only the degrees of freedom essential to describing the π-electron dynamics, thereby reducing the overhead associated with an exact treatment of interactions within the junction. Electron transport can then be treated using many-body Green's function techniques,[12,13] the Master equation approach,[14–18] or quantum impurity solvers.[19] This procedure begins with the observation that processes in systems of π-electrons take place at characteristic length, energy and time scales all ultimately dictated by the strength of the π-electron bond. Intuitively, one expects that only degrees of freedom with scales comparable to these need to be explicitly included. Semi-empirical models based on this notion have been in use for over fifty years,[20–23] and work to improve their accuracy is ongoing.[24–26] However, since these are based on ad hoc parameterizations[22,24–27] of interparticle Coulomb interactions that do not satisfy Maxwell's equations, it is difficult to extend such techniques to include effects like the screening of intramolecular interactions by the electrodes in molecular junctions.

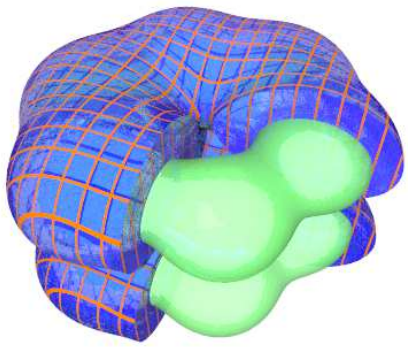

FIG. 1. Two isosurfaces of the average π-electron density $\langle\psi^\dagger(\vec{x})\psi(\vec{x})\rangle$ depict the electronic structure of gas-phase benzene within π-EFT.

In contrast to this, effective field theory (EFT) provides a concise, systematic method of constructing a π-electron Hamiltonian starting from first principles by per-

forming an expansion in a small parameter and then imposing symmetry constraints. The result contains a few physically meaningful parameters, which are then renormalized to include the aggregate effect of the degrees of freedom not explicitly retained. In this article we proceed along these lines, first expanding the full electronic Hamiltonian of a conjugated organic molecule in a basis of atomic orbitals and then dropping terms involving energies far from the π-electron bond energy.

Imposing symmetry constraints and performing an expansion in powers of the interatomic bond length then allows us to construct an effective Hamiltonian for the π-electrons in a conjugated organic molecule that accounts for the effects of σ-electrons virtually.[28] As an example of this, we consider the particular case of gas-phase benzene, for which we formulate an effective Hamiltonian with only four adjustable parameters: the on-site repulsion U, the nearest-neighbor hopping matrix element t, a dielectric constant ϵ, and the π-electron quadrupole moment Q. In principle, these could then be renormalized ab initio, e.g. by using perturbation theory to freeze out degrees of freedom far from the π-electron energy scale; however, since this is tedious and would not enhance the predictive power of our model, we instead fit the parameters directly to experiment.

Next, we show how screening from metallic electrodes can be incorporated into this scheme without introducing additional parameters by considering the multipole moments of image charge distributions. We then use this method of screening to calculate the screened HOMO-LUMO gap of benzene near a metallic electrode, as well as to formulate a realistic model of a gold-benzenedithiol-gold junction, including effects arising from the presence of the thiol sidegroups. The differential conductance spectrum of the junction is calculated as a function of the gate and bias voltages in the experimentally relevant regime,[30] exhibiting the characteristic diamond-shaped features[12] indicative of quantized charge on the molecule within the junction. Finally, we also use this π-electron effective field theory (π-EFT) to compute the π-electron contribution to the van der Waals interaction between benzene and a metallic electrode.

II. BARE HAMILTONIAN

Using the Born-Oppenheimer approximation, the one-body term in the electronic Hamiltonian for an isolated molecule can be written as

$$H^{(1)} = \sum_{\sigma} \int d^3x\, \psi^{\dagger}_{\sigma}(\vec{x}) \left(\frac{-\hbar^2}{2m}\nabla^2 + V \right) \psi_{\sigma}(\vec{x}) \qquad (1)$$

where V is the interaction between the electrons and the atomic nuclei. The operator that creates an electron with spin σ in the nth element of a basis of atomic orbitals $\{\phi_n\}$ can be expressed as:

$$d^{\dagger}_{n\sigma} = \int d^3x\, \phi_n(\vec{x}) \psi^{\dagger}_{\sigma}(\vec{x})$$

Multiplying this by the inverse of the overlap matrix $S_{nm} = \langle \phi_n | \phi_m \rangle$ and summing over m implies

$$\sum_m d^{\dagger}_{n\sigma} S^{-1}_{nm} \phi^*_m(\vec{x}) = \int d^3x' \sum_m \phi_n(\vec{x}') S^{-1}_{nm} \phi^*_m(\vec{x}) \psi^{\dagger}_{\sigma}(\vec{x}') = \psi^{\dagger}_{\sigma}(x) \qquad (2)$$

where we have made use of the completeness relation for a non-orthogonal basis:[31]

$$\sum_{nm} \phi_n(\vec{x}') S^{-1}_{nm} \phi^*_m(\vec{x}) = \delta(\vec{x} - \vec{x}')$$

Combining equations (1) and (2) then gives:

$$H^{(1)} = \sum_{nm\sigma} \mathcal{H}_{nm} d^{\dagger}_{n\sigma} d_{m\sigma} \qquad (3)$$

where

$$H^{(1)}_{nm} = \int d^3x\, \phi^*_n(\vec{x}) \left(\frac{-\hbar^2}{2m}\nabla^2 + V \right) \phi_m(\vec{x}) \qquad (4)$$

and

$$\mathcal{H}_{nm} = \sum_{kl} S^{-1}_{nk} H^{(1)}_{kl} (S^{-1}_{ml})^*. \qquad (5)$$

If we keep only nearest-neighbor terms this reduces to the Hückel Hamiltonian

$$H^{(1)} = \sum_n \varepsilon_n d^{\dagger}_{n\sigma} d_{n\sigma} - \sum_{\langle n,m \rangle, \sigma} t_{nm} d^{\dagger}_{n\sigma} d_{m\sigma}$$

where $t_{nm} = \mathcal{H}^{(1)}_{nm}$ and $\varepsilon_n = \mathcal{H}^{(1)}_{nn}$.

Similarly, the two-body term in the electronic Hamiltonian can be written as

$$H^{(2)} = \frac{1}{2} \sum_{\sigma\sigma'} \int d^3x_1 d^3x_2\, \psi^{\dagger}_{\sigma}(\vec{x}_1) \psi^{\dagger}_{\sigma'}(\vec{x}_2) \frac{e^2}{|\vec{x}_1 - \vec{x}_2|} \times \psi_{\sigma'}(\vec{x}_2) \psi_{\sigma}(\vec{x}_1),$$

which, in terms of the atomic orbital basis, is equivalent to

$$H^{(2)} = \frac{1}{2} \sum_{nmlk\sigma\sigma'} \mathcal{U}_{nmlk} d^{\dagger}_{n\sigma} d^{\dagger}_{m\sigma'} d_{l\sigma'} d_{k\sigma} \qquad (6)$$

where

$$U_{nmkl} = \int d^3x_1 d^3x_2\, \phi^*_n(\vec{x}_1) \phi^*_m(\vec{x}_2) \frac{e^2}{|\vec{x}_1 - \vec{x}_2|} \times \phi_k(\vec{x}_2) \phi_l(\vec{x}_1)$$

and

$$\mathcal{U}_{nmkl} = \sum_{opqr} S^{-1}_{no} S^{-1}_{mp} U_{opqr} (S^{-1}_{kq})^* (S^{-1}_{lr})^*. \qquad (7)$$

Together, equations (3)-(5) and (6)-(7) give the full electronic Hamiltonian from first principles:

$$H = H^{(1)} + H^{(2)},$$

but do so in terms of a basis that is impractically large for use within existing many-body techniques. To overcome this difficulty, in the next section we formulate an effective Hamiltonian in a reduced basis, explicitly retaining only the degrees of freedom necessary to describe the π-electron dynamics.

III. EFFECTIVE HAMILTONIAN

The first step in constructing the effective Hamiltonian is culling elements of the basis that lie far from the energy scale of interest. To this end, we first exclude atomic orbitals that do not participate in chemical bonding (those corresponding to core or excited electrons), which, in a π-electron system, leaves an effective s orbital and three effective p orbitals at each atom. The former hybridize with the effective p_x and p_y orbitals giving rise to three sp^2 hybrids that form the σ bonds between the atoms. The remaining effective p_z orbitals, which, for a planar molecule, cannot hybridize with any of the σ-electrons without breaking inversion symmetry, are occupied by one electron on each atom and form π bonds with weaker binding energies. Because of this energy difference we also omit the atomic orbitals participating in the σ bonds, though this approximation could be relaxed at the expense of a larger basis.

The effective Hamiltonian for the remaining effective p orbitals can then be determined using equations (3) through (7) if the effective orbitals are known. In principle, these could be calculated directly, e.g. by using perturbation theory to freeze out the degrees of freedom far from the π-electron energy scale; however, as noted previously we find it more practical to parametrize these expressions by imposing symmetry constraints.

To do this, we work initially in the asymptotic limit where the interatomic bond length is large compared to the size of the effective orbitals. This condition implies that matrix elements U_{nmkl} with $n \neq l$ or $m \neq k$ and overlap integrals S_{nm} with $n \neq m$ are exponentially small, allowing us to reduce the interaction matrix (Eq. (7)) to

$$\begin{aligned}\mathcal{U}_{nmkl} &= U_{nmkl} \\ &= \delta_{nl}\delta_{mk}\int d^3x_1 d^3x_2 \, \frac{e^2|\phi_n(\vec{x}_1)|^2|\phi_m(\vec{x}_2)|^2}{|\vec{x}_1 - \vec{x}_2|} \\ &\equiv \delta_{nl}\delta_{mk}U_{nm} \end{aligned} \tag{8}$$

where ϕ_n are now effective instead of bare orbitals. Although it is known[22] that the terms neglected are not a priori negligible at typical interatomic distances, it has been suggested that this approximation can be justified by the use of orthogonalized orbitals,[32] and it has been explicitly shown[33] that this is an accurate approximation for π-conjugated systems. Here we offer a simpler perspective more consistent with the spirit of EFT, namely that the neglected terms are accounted for virtually when the parameters in the Hamiltonian are renormalized. We also note that Eq. (8) is equivalent to the "neglect of differential overlap approximation" that has already been used extensively elsewhere, but that in the context of EFT it is simply the requirement that the effective Hamiltonian be local. However, we note here that in order to extend the present work to the case where multiple orbitals (e.g. both σ and π) are centered on the same atom, it would be necessary to include the same-site interaction matrix elements as additional parameters.

Expanding Eq. (8) in powers of the interatomic bond length yields a standard electrostatic multipole expansion, and, if we assume the effective p orbitals possess azimuthal and inversion symmetry, U_{nm} can be parametrized up to the quadrupole-quadrupole interaction in terms of the on-site repulsion U_{nn} and the zz component of the quadrupole moment Q_n associated with each orbital, as well as a dielectric constant ϵ included to account for the polarizability of the σ and core electrons.

Explicitly, this gives

$$\begin{aligned} U_{nm} &= U_{nn}\delta_{nm} \\ &\quad + (1-\delta_{nm})\left(U^{MM}_{nm} + U^{QM}_{nm} + U^{QM}_{mn} + U^{QQ}_{nm}\right) \\ &\quad + O(r^{-6}), \end{aligned} \tag{9}$$

where U^{MM} is the monopole-monopole interaction, U^{QM} is the quadrupole-monopole interaction, and U^{QQ} is the quadrupole-quadrupole interaction. For two orbitals with arbitrary quadrupole moments Q^{ij}_n and Q^{kl}_m separated by a displacement $\vec{r}$, the expressions for these are

$$U^{MM}_{nm} = \frac{e^2}{\epsilon r} \tag{10}$$

$$U^{QM}_{nm} = \frac{-e}{2\epsilon r^3}\sum_{ij} Q^{ij}_m \hat{r}_i \hat{r}_j \tag{11}$$

$$U^{QM}_{mn} = \frac{-e}{2\epsilon r^3}\sum_{ij} Q^{ij}_n \hat{r}_i \hat{r}_j \tag{12}$$

$$U^{QQ}_{nm} = \frac{1}{12\epsilon r^5}\sum_{ijkl} Q^{ij}_n Q^{kl}_m W_{ijkl}, \tag{13}$$

where

$$\begin{aligned} W_{ijkl} &= \delta_{li}\delta_{kj} + \delta_{ki}\delta_{lj} - 5r^{-2}(r_k\delta_{li}r_j + r_k r_i \delta_{lj} \\ &\quad + \delta_{ki}r_j r_l + r_i\delta_{kj}r_l + r_k r_l \delta_{ij}) + 35 r^{-4} r_i r_j r_l r_k \end{aligned}$$

is a rank-four tensor that characterizes the interaction of two quadrupoles.[34] Altogether, this provides an expression for the interaction energy that is correct up to fifth order in the interatomic distance.

To further reduce the number of free parameters it is convenient to simplify the effective Hamiltonian by requiring it to satisfy particle-hole symmetry. Although this is not strictly necessary within the context of π-EFT, the success of Pariser-Parr-Pople type semi-empirical models–which implicitly assume particle-hole symmetry–suggests that it is a good approximation to do so. Taking this to be the case, Eq. (4) then gives for the one-body

Hamiltonian:

$$H^{(1)}_{nm} = \int d^3x\, \phi^*_n(\vec{x}) \left(\frac{-\hbar^2}{2m}\nabla^2 + \sum_l V_l(\vec{x}) \right) \phi_m(\vec{x}),$$

where $V_l(\vec{x})$ is the effective potential due to the ionic hole at site l:

$$V_l(\vec{x}) = \int d^3x' \, \frac{-e^2|\phi_l(\vec{x}')|^2}{\epsilon|\vec{x}-\vec{x}'|}.$$

Using Eq. (8) then gives

$$H^{(1)}_{nm} = \delta_{nm} \left(\varepsilon^{(at)}_n - \sum_{l\neq n} U_{nl} \right) + (1-\delta_{nm}) t_{nm},$$

where we have defined the atomic on-site energy as:

$$\varepsilon^{(at)}_n = \int d^3x\, \phi^*_n(\vec{x}) \left(\frac{-\hbar^2}{2m}\nabla^2 + V_n(\vec{x}) \right) \phi_n(\vec{x}).$$

Defining $\rho_n = \sum_\sigma d^\dagger_{n\sigma} d_{n\sigma}$ and rearranging the two-body term then yields:

$$\begin{aligned} H^{(1)} + H^{(2)} = &\sum_n \varepsilon^{(at)}_n \rho_n - \sum_{\langle n,m\rangle,\sigma} t_{nm} d^\dagger_{n\sigma} d_{m\sigma} \\ &+ \frac{1}{2}\sum_{nm} U_{nm}(\rho_n - 1)(\rho_m - 1) \\ &+ \frac{1}{2}\sum_n U_{nn}\rho_n - \frac{1}{2}\sum_{nm} U_{nm}. \end{aligned}$$

Finally, adding the mutual repulsion of the ionic cores $\frac{1}{2}\sum_{n\neq m} U_{nm}$ gives the full effective molecular Hamiltonian:

$$\begin{aligned} H = &\sum_n \varepsilon^{(at)}_n \rho_n - \sum_{\langle n,m\rangle,\sigma} t_{nm} d^\dagger_{n\sigma} d_{m\sigma} \\ &+ \frac{1}{2}\sum_{nm} U_{nm} q_n q_m \\ &+ \frac{1}{2}\sum_n U_{nn} q_n, \end{aligned}$$

where we have introduced the effective charge operator defined by $q_n = \rho_n - 1$. In conjunction with Eq. (9), this expresses the effective Hamiltonian for an arbitrary π-electron system in terms of the tight-binding matrix t_{nm}, the on-site repulsion U_{nn}, a dielectric constant ϵ, and the π-electron quadrupole moment Q_n.

In the remainder of this paper we focus on benzene as a benchmark system, in which case the Hamiltonian reduces to

$$H = \mu \sum_n \rho_n - t \sum_{\langle n,m\rangle,\sigma} d^\dagger_{n\sigma} d_{m\sigma} + \frac{1}{2}\sum_{nm} U_{nm} q_n q_m, \quad (14)$$

where $U_{nn} = U$ and $Q^{zz}_n = -Q^{xx}_n/2 = -Q^{yy}_n/2 \equiv Q$ by symmetry. The molecular chemical potential μ is fixed by the experimental ionization energy[35–39] and electron affinity:[40]

$$\mu = \frac{IE - EA}{2} = -4.06 \text{ eV},$$

whereas the four other parameters must be renormalized by fitting to experiment, which is the subject of the following section.

IV. RENORMALIZATION: FITTING THE GAS-PHASE SPECTRUM

We have renormalized the parameters in our effective Hamiltonian for gas-phase benzene by fitting to experimental values that should be accurately reproduced within a π-electron only model. In particular, we have simultaneously optimized the theoretical predictions of 1) the vertical ionization energy, 2) the vertical electron affinity, and 3) the six lowest singlet and triplet excitations of the neutral molecule.

This was done by exactly diagonalizing Eq. (14) with the interatomic bond length[45] fixed at 1.40 Å. In particular, using the OQNLP algorithm[46] for nonlinear global optimization we minimized the RMS relative error of our predictions for the quantities in the first column of Table I. The results of this procedure, which converged to the same solution regardless of initial conditions, are summarized in column two of the same table. The optimal parametrization for the π-EFT was found to be $t = 2.70$ eV, $U = 9.69$ eV, $Q = -0.65$ eÅ^2 and $\epsilon = 1.56$ with a RMS relative error of 4.2 percent.

Also appearing in Table I are the predictions of a recent Pariser-Parr-Pople type semi-empirical model[26] as well as those of the original Ohno parametrization.[22,27] Compared to the recent PPP model, π-EFT fits the optical spectrum of gas-phase benzene to a similar degree of accuracy and gives better results for the ionization energy and electron affinity. Moreover, the parameters common to both models have comparable values, namely those given above for our model and those of the model of Castleton et al.[26] ($t = 2.64$ eV, $U = 8.9$ eV, and $\epsilon = 1.28$). The π-EFT on-site repulsion is also in qualitative agreement with recent RPA-based calculations of the effective Coulomb repulsion in graphene.[47]

Although our effective quadrupole moment has no direct counterpart in phenomenological models, its value can be compared to the bare quadrupole moment of a hydrogenic $2p_z$ orbital, which is given by

$$Q_{zz} = -24e(a_0/Z)^2, \quad (15)$$

where a_0 is the Bohr radius and $+Ze$ is the nuclear charge. Using this, we find that our π-orbital quadrupole moment corresponds to a hydrogenic p orbital bound by an effective charge of $+3.22e$, or, equivalently, with an effective Bohr radius of 0.16 Å. This is consistent with the expectation that the sp^2 orbitals forming the σ bonds

	Exp.[35–44]	π-EFT	PPP Castleton et. al[26]	PPP Ohno[22,27]
Ionization Energy (eV)	9.23	9.26	9.05	9.78
Electron Affinity (eV)	-1.12	-1.14	-0.93	-1.67
Neutral Spectrum (eV)				
Singlet	4.90	4.87	4.76	4.23
	6.21	6.08	6.30	5.52
	6.93	7.59	6.93	6.81
Triplet	3.93	4.10	3.99	3.52
	4.75	4.92	4.74	4.32
	5.60	6.17	5.84	5.58
RMS Relative Error (%)	N/A	4.2	6.0	19.0

TABLE I. Experimental data for the vertical ionization energy,[35–39] vertical electron affinity,[40] and optical spectrum,[41–44] of gas-phase benzene compared to the predictions of π-EFT, a recent PPP-type model,[26] and the Ohno parametrization.[22,27] The best fit parameterization of our π-EFT was determined to be $t = 2.70$ eV, $U = 9.69$ eV, $Q = -0.65\ e\text{Å}^2$ and $\epsilon = 1.56$.

provide only weak screening of the atomic core, which has a net charge of +4e. For the purpose of visualization, effective hydrogenic orbitals can also be used to render the average π-electron density $\langle\psi^\dagger(\vec{x})\psi(\vec{x})\rangle$, as shown in Figure 1.

V. SCREENING BY METALLIC ELECTRODES: THE IMAGE MULTIPOLE METHOD

In this section, we extend the preceding model to include the effect of screening by metallic electrodes, which for simplicity are modeled as planar or spherical conductors. In the regime where the characteristic response time of the electrons in the electrode is much shorter than the timescale of the π-electron dynamics, this can be done using the method of images via a straightforward extension of Eq. (9). This is expected to be the case for conjugated organic molecules in the vicinity of gold electrodes, in which case the metallic plasma frequency[48] $\omega_p \approx 9$ eV/$\hbar$ is large compared to the frequency scale of π excitations $\omega_\pi \approx 2t/\hbar \approx 5$ eV/$\hbar$. The leading order correction to the metallic dielectric function, given by the GW approximation, then goes as $(\omega_\pi/\omega_p)^2 \approx 0.3$. Explicit calculations using the GW approach also suggest that corrections to the image charge method tend to be small for organic molecules adsorbed on a metallic surface.[2]

In the following subsections, the multipole moments of the image charge distribution generated by an orbital near planar and spherical conductors are described. To determine the screened interaction matrix, interactions between these and the orbital multipole moments are included in U_{nm} using equations (10) through (13). Overall, the two-body Hamiltonian should give the energy required to prepare the molecular charge distribution by bringing each of the electrons in from infinity with the electrodes maintained at fixed electrostatic potentials. This can be ensured using a number of different counting schemes, but we take one that ensures a symmetric interaction matrix, namely

$$\tilde{U}_{nm} = U_{nm} + \delta_{nm}U^{(i)}_{nn} + \frac{1}{2}(1-\delta_{nm})(U^{(i)}_{nm} + U^{(i)}_{mn}),$$

where U_{nm} is the unscreened interaction matrix, $U^{(i)}_{nm}$ is the interaction between the nth orbital and the image of the mth orbital, and $\tilde{U}_{nm}$ is the screened interaction matrix. Since the image multipole moments of an orbital change as it is brought in from infinity, one might expect a prefactor of 1/2 in the second term of the preceding equation, however, this is already present in the Hamiltonian itself.

When multiple electrodes are present, the image of an orbital in one conductor produces images in the other electrodes, resulting in an effect reminiscent of a hall of mirrors. We deal with this by including these "higher order" multipole moments iteratively until the difference between successive approximations of $\tilde{U}_{nm}$ drops below a predetermined threshold. In practice, this procedure converged rapidly.

Within the foregoing scheme, the case where one or more electrodes are maintained at a fixed potential other than zero can be treated straightforwardly by including image charges that contribute to the one-body Hamiltonian rather than to $\tilde{U}_{nm}$. For example, a spherical contact with radius R at potential V can be treated using a hypothetical point charge $q = VR$ at the center of the electrode. This technique is especially useful for transport calculations in the context of molecular junctions, as it provides the full junction Hamiltonian at finite bias, alleviating the need for the phenomenological models of capacitive lead-molecule coupling that have been relied upon on in the past.[12]

A. Screening by a planar electrode

In classical electrostatics, the image of a charge distribution near a planar conductor is merely the mirror image of the charge distribution itself. Thus an orbital with monopole moment q and quadrupole moment Q^{ij} located a distance r away from a conducting plane produces an image orbital inside the conductor located at depth r with multipole moments $\tilde{q} = -q$ and $\tilde{Q}^{ij} = -\sum_{kl} T_{ik}T_{jl}Q^{kl}$, where T_{ik} is a transformation matrix representing a reflection about a plane parallel to the surface of the conductor, i.e.

$$T_{ik} = \delta_{ik} - 2\hat{n}_i\hat{n}_k, \tag{16}$$

where $\hat{n}$ is the unit vector normal to the planar surface.

B. Screening by a spherical electrode

An orbital with monopole moment q and quadrupole moment Q^{ij} located a distance r from the center of a spherical electrode with radius R induces an image distribution at $\tilde{r} = R^2/r$ with monopole and quadrupole moments

$$\tilde{q} = -q\frac{R}{r} - \frac{R}{2r^3}\sum_{ij} Q^{ij}\hat{r}_i\hat{r}_j$$

and

$$\tilde{Q}^{ij} = -\left(\frac{R}{r}\right)^5 \sum_{kl} T_{ik}T_{jl}Q^{kl}$$

respectively, where T_{ik} is a transformation matrix representing a reflection about the plane normal to the vector $\hat{r}$, similar to Eq. (16).

Thus the orbital quadrupole moment induces a higher order image monopole moment, as well as an image of itself that is deformed and reflected. An image dipole is also generated, but its interaction with the orbital charge distribution is of order r^{-7} and so we have neglected it here.

VI. SCREENING OF THE HOMO-LUMO GAP

Although π-EFT could be used to study a wide variety of phenomena involving conjugated organic molecules, our primary motivation in formulating it has been to facilitate realistic many-body calculations of transport phenomena in molecular junctions. In particular, while recent semi-empirical models[26] reproduce the low-lying excitations of gas-phase benzene, their predictions of quantities relevant to transport, namely the fundamental (or HOMO-LUMO) gap and the optical excitations of the ionized molecule, are less accurate. Moreover, in a molecular junction these quantities are renormalized by screening from metallic electrodes as well as the presence of linker groups not explicitly included in the molecular Hilbert space.

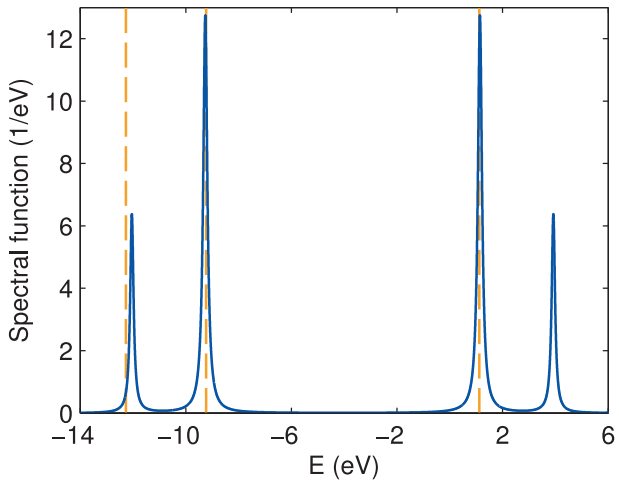

FIG. 2. The spectral function of gas-phase benzene broadened artificially as a guide to the eye. The dashed orange lines are fixed by (left to right) the lowest lying optical excitation of the molecular cation,[36–39,49] the vertical ionization energy of the neutral molecule,[35–39] and the vertical electron affinity of the neutral molecule.[40]

Within π-EFT these effects can be clearly seen: Consider the spectral function of gas-phase benzene, which we evaluate at the many-body level using the non-equilibrium Green's function formalism as described in appendix A. Figure 2 shows this quantity, along with experimental values for the vertical ionization energy (9.23 eV), vertical electron affinity (−1.12 eV), and the first optical excitation of the cation (3.04 eV). As a guide to the eye, the spectrum has been broadened artificially using a broadening matrix of $\Gamma_{nm} = (0.2\text{ eV})\delta_{nm}$. As an aside, we note here that the close agreement between the experimental values and the maxima of the spectral function suggests our model is accurate at this energy scale. In particular, the accuracy of the theoretical value for the lowest optical excitation of the cation is noteworthy, as this quantity was not fit during the renormalization procedure but rather represents a prediction of π-EFT.

Screening effects become evident when the molecule is brought into proximity with the surface of a planar electrode. Figure 3 shows the reduction of the ionization energy and electron affinity as a function of electrode-molecule distance in this scenario, and the HOMO-LUMO gap, given by $IE - EA$, is reduced commensurately. These results, based on the image multipole method, are also consistent with recent GW-based investigations of screening.[2,3]

We also considered the prototypical benzene-gold junction, consisting of benzene linked to two gold electrodes via thiol side groups. Although this junction can occur with a wide variety of different geometries, in this example we have taken the configuration shown in Fig-

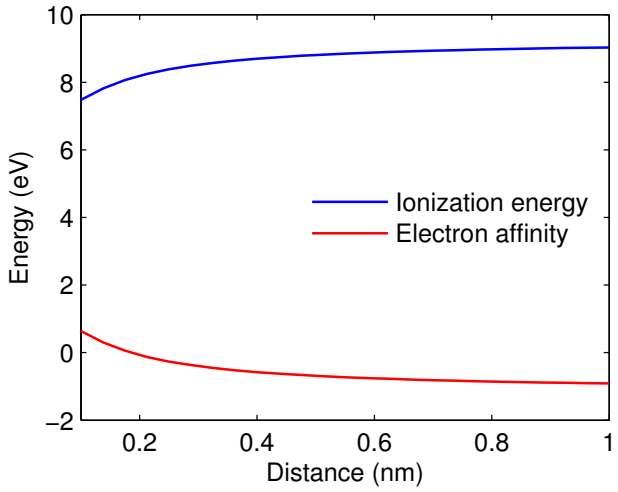

FIG. 3. The ionization energy and electron affinity of benzene oriented parallel to the surface of a screening plane, shown as a function of distance.

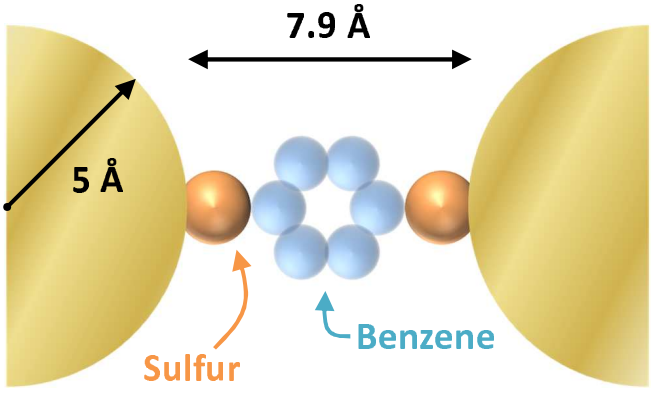

FIG. 4. The geometry[52,53] for the benzenedithiol junction associated with the spectral function shown in Figure 5. The electrodes have been placed so that the screening surface lies one covalent radius[54] beyond the position of the outermost gold nuclei, a convention that has been investigated elsewhere[55] in the context of atom-surface van der Waals interactions.

ure 4. The electrodes are modeled as metallic spheres with radii of 0.5 nm, and the partially ionic character of the gold-sulfur bond has been accounted for by placing point charges of $-0.67e$ at the locations of the sulfur atoms. The latter value was determined in conjunction with the tunneling-width matrix ($\Gamma_{11} = \Gamma_{44} = 0.44$ eV) via a simultaneous fit of the experimental thermopower[50] and conductance,[51] using the techniques described in appendix A. The upper panel of Figure 5 shows the spectral function for this junction in the simple case where the tunneling-width matrix is the same as in Figure 2, a choice which simplifies comparison of the two cases.

Screening from the electrodes reduces the HOMO-LUMO gap by 12.5 percent as compared to the gas-phase,

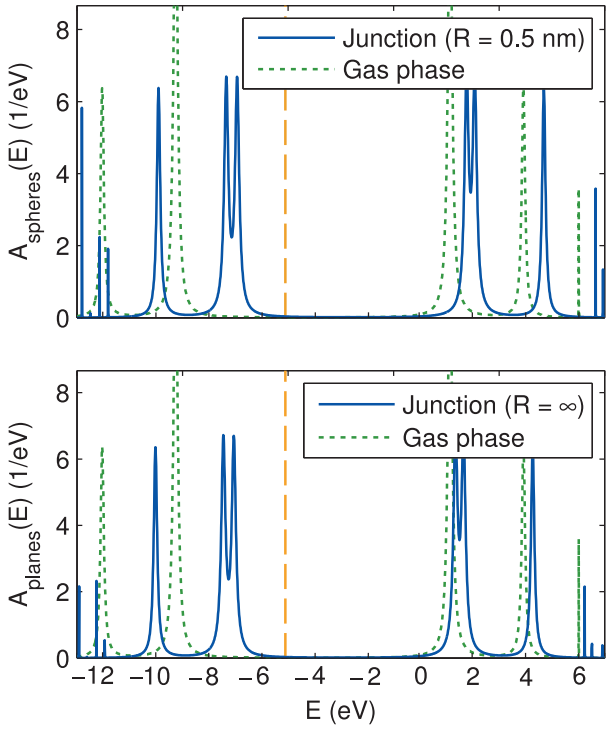

FIG. 5. Top: The spectral function of the Au-1,4-benzenedithiol-Au junction depicted in Figure 4 at room temperature, together with the gas-phase density of states from Figure 2. To facilitate comparison, the same broadening has been used in both cases. The dotted orange line at -5.1 eV indicates the position of the experimental chemical potential of clean gold.[56] Bottom: The spectral function of the same junction with planar instead of spherical electrodes.

and the dipole formed by the gold-sulfur bond shifts the chemical potential of the molecule up by 1.4 eV. For comparison, we have also calculated the spectral function of the same junction, but with the electrodes modeled as planes (Figure 5, bottom), in which case the screening is maximal and the HOMO-LUMO gap is reduced by 19 percent. These results are qualitatively consistent with GW-based investigations of screening effects wherein a molecule is adsorbed on a metallic surface,[2,3] as well as with the recent state-of-the-art GW calculations for benzenedithiol-Au junctions.[11] In comparison to Ref. 11, the HOMO and LUMO resonances in Fig. 5 are both shifted slightly upward in energy, but the gap between them is comparable. It should be pointed out that the upward shifts of HOMO and LUMO in our model are due in part to the dipole moments of the S-Au bonds, which are treated phenomenologically in our model, while the screening of the HOMO-LUMO gap is a fundamental effect described by the image multipole method. As compared to models of screening that treat only the π-orbital monopole moment,[57] the reduction of the HOMO-LUMO gap predicted herein is somewhat smaller, presumably owing to the tendency of the monopole-quadrupole and

quadrupole-quadrupole interactions to soften short-range Coulomb interactions. For both of the electrode geometries we considered, a splitting of the two-fold degenerate HOMO and LUMO resonances can also be seen, which arises from the interaction between the π-electrons and the dipoles associated with the partly ionic gold-sulfur bonds.

We also note that, as compared to DFT-based treatments of similar junctions,[58] the HOMO-LUMO gap seen in Figure 5 is dramatically larger, consistent with the observation[59] that correlation effects beyond the scope of local DFT must be included to accurately model transport through this junction.

VII. DIFFERENTIAL CONDUCTANCE SPECTRUM

The advantages of a computational approach such as π-EFT combined with many-body NEGF are perhaps most evident in describing transport through a molecular junction far from equilibrium.[30,60–62] For then, not only must the equilibrium energetics of electron addition and removal be described correctly, but the dependence of both processes on both gate and bias voltages must be correct, a significant challenge for conventional approaches.[10] To illustrate the advantages of π-EFT in this context, we have calculated the differential conductance spectrum of a Au-1,4-benzenedithiol-Au junction. Figure 6 shows the absolute value of the differential conductance on a logarithmic scale, calculated as a function of bias voltage and the electrostatic potential on a spherical gate electrode of radius 3Å centered 5Å above the benzene ring. The effective electrostatic lever arm of the gate is 0.21eV/V. The junction geometry is otherwise identical to that depicted in Fig. 4. In Fig. 6, we have used the physical tunneling-width matrix $\Gamma_{11} = \Gamma_{44} = 0.44$ eV.

Of particular note are the diamond-shaped features in the differential conductance spectrum: the charge on the molecule within the junction is quantized and the differential conductance is suppressed within the diamond-shaped regions centered along the horizontal axis due to the phenomenon of Coulomb blockade.[10,12] This is similar to what has been observed experimentally in junctions based on larger dithiolated molecules,[60–62] in which case the charging energy is significantly smaller. To describe this phenomenon within DFT would require a proper treatment of the derivative discontinuity[8,9] far from equilibrium, for which no theory currently exists. To the best of our knowledge, charge quantization effects like these are beyond the scope even of self-consistent many-body perturbation theory, e.g. as in the case of the state-of-the-art DFT + GW approach.[11]

Resonant tunneling through electronic excited states at large bias and suppression of transport at small bias due to destructive quantum interference (blue fringes) are also clearly visible in Fig. 6. This differential conductance spectrum is similar to that obtained previously[12] using a PPP model of the electronic structure. The main differences are that the sizes of the Coulomb diamonds are reduced due to screening from the metal electrodes, and the particle-hole symmetry of the PPP spectrum is broken by the presence of the S-Au dipoles.

VIII. π-ELECTRON CONTRIBUTION TO THE VAN DER WAALS INTERACTION

As a final application of the image-multipole method, we consider the π-electron contribution to the van der Waals interaction between a molecule and a metallic electrode. Experimentally, such interactions are important when a molecule is adsorbed on a metal surface, or in single-molecule junctions in which a molecule bonds directly to metallic electrodes, as in the Pt-benzene-Pt junctions investigated recently by Kiguchi et al.[63] Theoretically, the van der Waals interaction also represents a unique challenge in that it is a true many-body phenomenon arising from quantum correlations induced by long-range interactions. As such, it is outside the scope of local approximations to density functional theory, and modeling van der Waals interactions using nonlocal functionals is a topic of ongoing research.[64–66] In contrast to this, the preceding treatment of screening, in conjunction with a full many-body treatment of the π-electrons on the molecule, makes it possible to calculate the π-electron contribution to van der Waals interaction straightforwardly with no extra adjustable parameters.

In particular, by exactly diagonalizing the few-body molecular Hamiltonian with and without the effects of screening included in U_{nm}, it is possible to infer the van der Waals interaction at zero temperature between a molecule and a metallic electrode by comparing the expectation values of the Hamiltonian in these two cases:

$$E_{vdW} = \langle \tilde{H} \rangle - \langle H \rangle$$

This procedure was carried out at zero temperature for benzene oriented parallel to the surface of a spherical electrode over a large range of electrode-molecule distances, and the results are shown in Figure 7. When the molecule is near the surface of the electrode $E_{vdW} = -\frac{C_3}{r^3}$, which is the expected asymptotic dependence for the van der Waals interaction between a molecule and a planar conductor. Conversely, when the molecule is far from the electrode $E_{vdW} = -\frac{C_6}{r^6}$, which is the usual asymptotic dependence of the van der Waals interaction as given by the Lennard-Jones potential. A clear transition between the two regimes can be seen around 10 nm, the radius of the electrode. In the near-field region the constant of proportionality predicted by π-EFT is $C_3 \approx 1.56$ eV Å^3. We also investigated the orientation dependence of the van der Waals interaction between a planar electrode and a benzene molecule, as depicted in Figure 8, which shows a significantly stronger attractive interaction when the plane of the molecule is oriented perpendicular to the surface of the electrode.

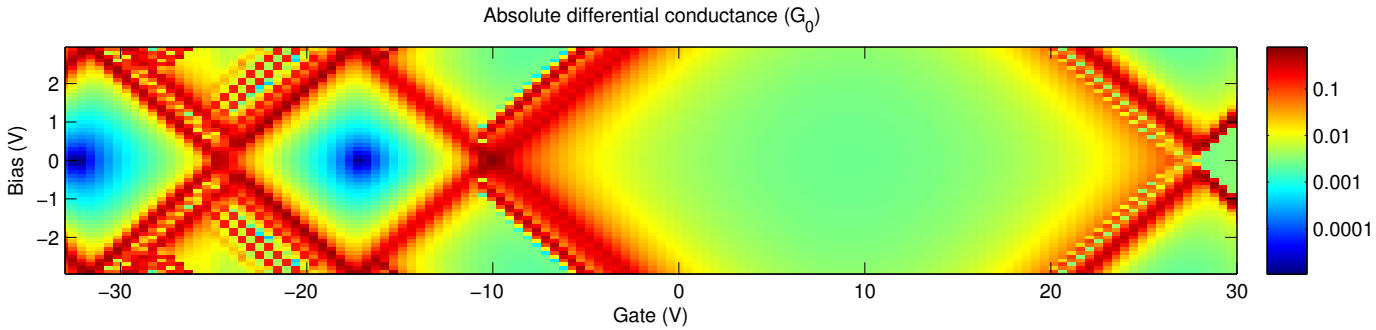

FIG. 6. Differential conductance spectrum of a Au-1,4-benzenedithiol-Au junction at room temperature versus gate and bias voltages. The junction geometry, including source and drain electrodes, is depicted in Fig. 4; a spherical gate electrode of radius 3Å (not shown) is centered 5Å above the benzene ring. The effective electrostatic lever arm of the gate is 0.21eV/V. The charge on the molecule within the junction is quantized within the diamond-shaped regions centered on the horizontal axis due to the phenomenon of Coulomb blockade. Resonant tunneling through electronic excited states at large bias and suppression of transport at small bias due to destructive quantum interference (blue fringes) are clearly visible.

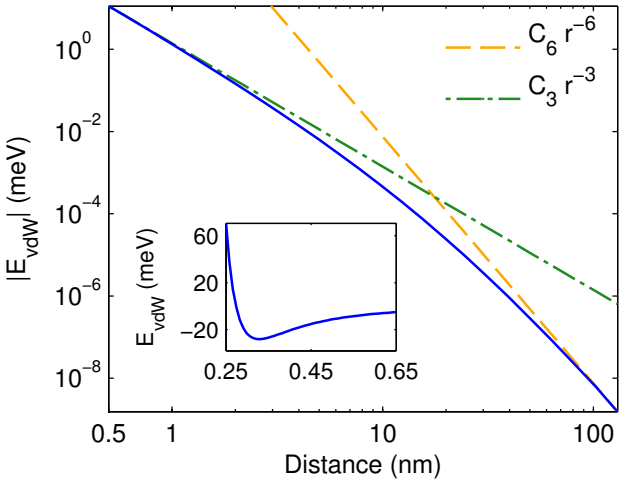

FIG. 7. The π-electron contribution to the van der Waals interaction between benzene and a spherical electrode with a radius of 10 nm, plotted as a function of the distance from the conducting surface. At all distances the molecule is oriented parallel to the surface of the electrode. The dashed green and orange lines show the expected asymptotic dependence in the near and far fields respectively. Inset: The same quantity very near the surface of the electrode, including a phenomenological[67] gold-carbon hard-core repulsion.

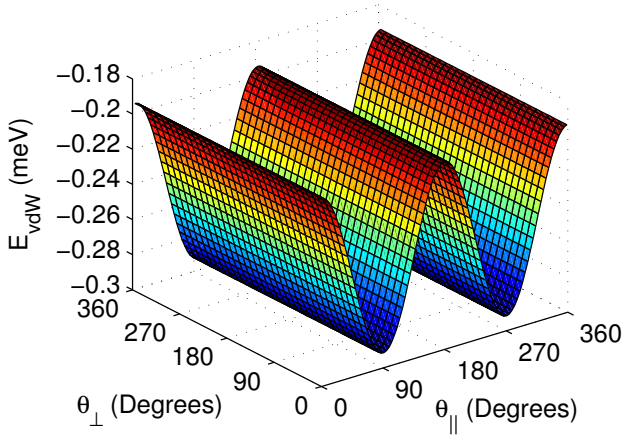

FIG. 8. The orientation dependence of the π-electron contribution to van der Waals interaction between a planar electrode and a benzene molecule centered 2 nm from the metal surface. The molecule is initially oriented parallel to the electrode and then rotated by an angle $\theta_\perp$ about the axis perpendicular to the plane of the molecule, followed by a rotation of $\theta_\parallel$ about an axis within the plane of the molecule.

The van der Waals coefficient C_3 is fundamentally related to the molecular polarizability tensor α_{ij}. Thus, for an axially symmetric molecule such as benzene, a simplified single-oscillator model can be used to derive semi-empirical formulae relating α_{ij} to C_3 with the molecule oriented either parallel or perpendicular to the surface of a planar electrode:[68]

$$C_3^{\parallel} \approx \frac{E_d}{32}(2\alpha_\perp + 2\alpha_\parallel) \tag{17}$$

$$C_3^{\perp} \approx \frac{E_d}{32}(\alpha_\perp + 3\alpha_\parallel) \tag{18}$$

Here E_d is the energy of the principal dipole-allowed optical transition, and $\alpha_\parallel$ and $\alpha_\perp$ are respectively the molecular polarizabilities parallel and perpendicular to its plane of symmetry. As an internal consistency check and to demonstrate that our technique captures the basic physics of the van der Waals interaction, we have calculated these quantities within π-EFT ($E_d = 7.59$ eV, $\alpha_\parallel = 3.24$ Å^3 and $\alpha_\perp = 0.00$ Å^3), and used them to deduce $C_3^{\parallel} \approx 1.54$ eV·Å^3 and $C_3^{\perp}/C_3^{\parallel} = 1.5$, which are in close agreement with the values of C_3 obtained via direct calculation.

Experimentally, $\alpha_\parallel = 12.31$ Å^3, $\alpha_\perp = 6.35$ Å^3 and $E_d = 6.93$ eV for benzene, and in this case Eq. (17) gives $C_3^{\parallel} \approx 8.08$ eV Å^3, which is roughly five times larger than

that predicted by π-EFT. This discrepancy can be attributed to the significant contribution of the σ-electrons to the molecular polarizability, as evidenced by the large experimental value of $\alpha_\perp$, which arises from σ-π transitions. Consistent with this and the notion that all of the valence electrons contribute more or less equally to the molecular polarizability, the angular average of the π-EFT polarizability, i.e. $\frac{\alpha_\perp+2\alpha_\parallel}{3}$, is roughly a quarter of the same quantity calculated using experimental values. This underscores the importance of the σ-electron dynamics in the context of van der Waals interactions, which arise from the long-range spatial correlation of purely virtual processes. In contrast to this, the effect of the σ-electrons on real π-π transitions, such as those involved in transport, should be well described by π-EFT. Moreover, as noted previously, the σ-electrons dynamics can be explicitly included within effective field theory at the expense of a larger Hilbert space, and we believe that such a $\pi\sigma$-EFT would accurately reproduce the full van der Waals interaction between a conjugated molecule and a metallic electrode.

IX. CONCLUSIONS

We have shown how EFT can be used to provide a concise derivation of an effective Hamiltonian for π-electron systems by performing a multipole expansion, imposing symmetry constraints, and then renormalizing a few adjustable parameters. In particular, we have optimized the parameters appearing in an effective Hamiltonian for gas-phase benzene, Eq. (14), by fitting to experimental data for 1) the vertical ionization energy, 2) the vertical electron affinity, and 3) the six lowest singlet and triplet excitations of the neutral molecule. This procedure yields a fit which is comparable to or better than traditional PPP models[22,26,27], and gives $U = 9.69$ eV for the on-site repulsion, $t = 2.70$ eV for the nearest-neighbor hopping matrix element, $\epsilon = 1.56$ eV for the dielectric constant, and $Q = -0.65\ e\text{Å}^2$ for the π-electron quadrupole moment. These values of U, t, and ϵ are consistent with those used in previous π-electron models[26,27,47], while Q is a new physical parameter in our approach, which takes the place of the ad-hoc functional forms assumed in PPP models and governs the corrections to $1/r$ interactions at short distances.

We have also utilized π-EFT to model the screening of intramolecular Coulomb interactions by nearby metallic electrodes. Within our approach, lead-molecule coupling is treated using a two-step process wherein all long range Coulomb interactions are included nonperturbatively before lead-molecule tunneling is accounted for via Dyson's equation. The ability to include finite bias and screening effects via image multipoles–without additional adjustable parameters–represents a significant advantage of π-EFT over PPP models, which utilize interactions that do not satisfy Maxwell's equations.

In particular, we have shown how π-EFT facilitates a realistic description of the prototypical Au-1,4-benzenedithiol-Au junction, including transport far from equilibrium. The accurate description of ionization potential and electron affinity as poles of the Green's function—and their shifts due to interactions with metal electrodes, sets π-EFT apart from standard DFT-NEGF approaches, and promises to enable accurate transport calculations for junctions involving a variety of conjugated organic molecules. The ability to simultaneously describe Coulomb blockade and coherent quantum transport appears to set our approach apart even from state-of-the-art self-consistent many-body perturbation theory.[11] The main disadvantages of our approach compared to either DFT or DFT + GW are (i) that certain aspects of the junction are described only phenomenologically, such as the linker groups between the molecule and the metal electrodes; and (ii) that a full diagonalization even of the limited Hilbert space of the π-electrons scales very poorly. Nonetheless, exact diagonalization of π-EFT should be tractable for conjugated molecules significantly larger than benzene, such as biphenyl or triphenyl, and the use of configuration-interaction techniques such as coupled-cluster singles and doubles should allow its application to still larger molecules. For these systems, π-EFT provides a framework combining an accurate treatment of electron correlation with a higher degree of realism than is present in conventional PPP techniques.

ACKNOWLEDGMENTS

We thank Dr. Vincent Lonij for useful discussions. This material is based upon work supported by the Department of Energy under Award Number DE-SC0006699.

Appendix A: Many-body theory of transport in molecular junctions

Within the non-equilibrium Green's function approach to studying transport in molecular junctions, a quantity of central importance is the retarded Green's function G of the molecule coupled to the electrodes. In the energy domain and using matrix notation, this can be expressed via the Dyson equation as:

$$G = G_{mol} + G_{mol}\Sigma G, \tag{A1}$$

where G_{mol} is the interacting Green's function of the molecule without tunnel coupling to the electrodes, but including long-range Coulomb interactions between the π-electrons and their image multipole moments in the leads. The self-energy Σ can be partitioned into the tunneling self-energy Σ_T associated with the lead-molecule bonds, and a correction to the Coulomb self-energy $\Delta\Sigma_C$ arising from lead-molecule coherence:

$$\Sigma = \Sigma_T + \Delta\Sigma_C.$$

Far from resonance and at room temperature $\Delta\Sigma_C \approx 0$, and so in the present context we neglect this correction–an approximation which is justified in detail in ref. 12. Assuming the leads can be modeled as Fermi liquids with good screening, the electron-electron interactions within them can be neglected and the tunneling self-energy associated with a given electrode can be expressed as:[69]

$$\Sigma_T = V g(E) V^\dagger,$$

where $g(E)$ is the retarded Green's function of the lead and V_{nk} are the matrix elements coupling the lead and molecule. In the broad-band limit wherein the density of states in the electrodes varies slowly in the vicinity of the metallic Fermi level, the self-energy then reduces to a purely imaginary matrix with no energy dependence:[69]

$$\Sigma_T = -\frac{i}{2}\sum_\alpha \Gamma_\alpha. \tag{A2}$$

Here the tunneling-width matrix Γ_α associated with lead α given is by

$$\Gamma_{n\sigma,m\sigma} = 2\pi\rho(\varepsilon_f) V_n V_m^* \delta_{\sigma\sigma'},$$

where $\rho(\varepsilon_f)$ is the density of states at the metallic Fermi level, and V_n is the matrix element between the nth π-orbital in the molecule and the lead states in the vicinity of the Fermi level. The diagonal elements of this equation are equivalent to Fermi's golden rule, with $\mathrm{Tr}\,\{\Gamma_\alpha/\hbar\}$ giving the rate at which electrons in lead α are being injected into the molecule.

Aside from the self-energy, the other ingredient needed to evaluate Eq. (A1) is the Green's function of the isolated molecule. This is determined exactly by first finding the few-body eigenstates $\{|\nu\rangle\}$ and eigenenergies E_ν of the gas-phase molecule, and then using these to explicitly evaluate the molecular Green's function:[12,70]

$$G_{mol} = \sum_{\nu,\nu'} \frac{[P(\nu) + P(\nu')]\, C(\nu,\nu')}{E - (E_{\nu'} - E_\nu) + i0^+} \tag{A3}$$

Here $P(\nu)$ is the statistical occupancy of the νth eigenstate, given at equilibrium by the grand canonical ensemble, and

$$C_{n\sigma,m\sigma'}(\nu,\nu') = \langle\nu|d_{n\sigma}|\nu'\rangle\langle\nu'|d^\dagger_{m\sigma'}|\nu\rangle$$

are many-body matrix elements, where, in the present context, $d^\dagger_{m\sigma}$ creates an electron with spin σ in the mth π-orbital of the molecule.

Altogether, equations (A1), (A2) and (A3) provide a method for obtaining the full interacting Green's function of the molecule coupled to the electrodes, which may then be used to calculate the various physical quantities of interest. For example, the spectral function is given by:[69]

$$A(E) = -2\,\mathrm{Im}G,$$

the trace of which is proportional to the effective single-particle density of states:

$$\rho(E) = \frac{1}{2\pi}\mathrm{Tr}\,\{A\}$$

Similarly, the elastic transmission function between two electrodes can also be obtained from the full molecular Green's function via the expression:

$$T_{\alpha\beta} = \mathrm{Tr}\left\{\Gamma_\alpha G \Gamma_\beta G^\dagger\right\},$$

where Γ_α and Γ_β are the tunneling-width matrices associated with leads α and β respectively. This quantity may then be used to evaluate the various electronic transport quantities of interest,[71] such as the elastic electrical current

$$I^e_\alpha = \frac{-e}{h}\sum_\beta \int dE\; T_{\alpha\beta}\,(f_\beta - f_\alpha)$$

and elastic thermal current

$$I^Q_\alpha = \frac{1}{h}\sum_\beta \int dE\; (E-\mu_\alpha) T_{\alpha\beta}\,(f_\beta - f_\alpha)$$

flowing into lead α. Here $f_\alpha(E)$ and μ_α are respectively the Fermi-Dirac distribution and chemical potential associated with lead α.

* barr@physics.arizona.edu

[1] Juan Carlos Cuevas and Elke Scheer. *Molecular Electronics: An Introduction to Theory and Experiment*. World Scientific Publishing Company, 2010.

[2] J. B. Neaton, Mark S. Hybertsen, and Steven G. Louie. Renormalization of molecular electronic levels at metal-molecule interfaces. *Phys. Rev. Lett.*, 97(21):216405, Nov 2006.

[3] Kristian S. Thygesen and Angel Rubio. Renormalization of molecular quasiparticle levels at metal-molecule interfaces: Trends across binding regimes. *Phys. Rev. Lett.*, 102(4):046802, Jan 2009.

[4] C. Toher, A. Filippetti, S. Sanvito, and Kieron Burke. Self-interaction errors in density-functional calculations of electronic transport. *Phys. Rev. Lett.*, 95:146402, 2005.

[5] San-Huang Ke, H. U. Baranger, and Weitao Yang. Role of the exchange-correlation potential in *ab initio* electron transport calculations. *J. Chem. Phys.*, 126:201102, 2007.

[6] Aron J. Cohen, Paula Mori-Snchez, and Weitao Yang. Insights into current limitations of density functional theory. *Science*, 321(5890):792–794, 2008.

[7] C. Toher and S. Sanvito. Effects of self-interaction corrections on the transport properties of phenyl-based molecular junctions. *Physical Review B (Condensed Matter and Materials Physics)*, 77:155402, 2008.

[8] John P. Perdew, Robert G. Parr, Mel Levy, and Jose L. Balduz. Density-functional theory for fractional particle number: Derivative discontinuities of the energy. *Phys. Rev. Lett.*, 49:1691–1694, 1982.

[9] Justin P. Bergfield, Zhen-Fei Liu, Kieron Burke, and Charles A. Stafford. Bethe ansatz approach to the kondo effect within density-functional theory. *Phys. Rev. Lett.*, 108:066801, 2012.

[10] B. Muralidharan, A. W. Ghosh, and S. Datta. Conductance in Coulomb blockaded molecules–fingerprints of wave-particle duality? *Molecular Simulation*, 32(9):751–758, Aug 2006.

[11] M. Strange, C. Rostgaard, H. Häkkinen, and K. S. Thygesen. Self-consistent gw calculations of electronic transport in thiol- and amine-linked molecular junctions. *Phys. Rev. B*, 83:115108, Mar 2011.

[12] J. P. Bergfield and C. A. Stafford. Many-body theory of electronic transport in single-molecule heterojunctions. *Phys. Rev. B*, 79(24):245125, Jun 2009.

[13] J. Rincón, K. Hallberg, and A. A. Aligia. Quantum interference in coherent molecular conductance. *Phys. Rev. Lett.*, 103:266807, 2009.

[14] Jürgen König, Herbert Schoeller, and Gerd Schön. Cotunneling at resonance for the single-electron transistor. *Phys. Rev. Lett.*, 78:4482–4485, 1997.

[15] Herbert Schoeller and Jürgen König. Real-time renormalization group and charge fluctuations in quantum dots. *Phys. Rev. Lett.*, 84:3686–3689, 2000.

[16] Jonas Nyvold Pedersen and Andreas Wacker. Tunneling through nanosystems: Combining broadening with many-particle states. *Phys. Rev. B*, 72:195330, 2005.

[17] U. Harbola and S. Mukamel. Superoperator nonequilibrium green's function theory of many-body systems; applications to charge transfer and transport in open junctions. *Physics Reports*, 465(5):191 – 222, 2008.

[18] M. Galperin, A. Nitzan, and M. A. Ratner. Inelastic transport in the Coulomb blockade regime within a nonequilibrium atomic limit. *Phys. Rev. B*, 78:125320, 2008.

[19] D. Bohr, P. Schmitteckert, and P. Wölfle. DMRG evaluation of the kubo formula conductance of strongly interacting quantum systems. *EPL (Europhysics Letters)*, 73(2):246, 2006.

[20] Rudolph Pariser and Robert G. Parr. A semi-empirical theory of the electronic spectra and electronic structure of complex unsaturated molecules. ii. *The Journal of Chemical Physics*, 21(5):767–776, 1953.

[21] Robert G. Parr. Three remarks on molecular orbital theory of complex molecules. *The Journal of Chemical Physics*, 33(4):1184–1199, 1960.

[22] Kimio Ohno. Some remarks on the pariser-parr-pople method. *Theoretical Chemistry Accounts: Theory, Computation, and Modeling (Theoretica Chimica Acta)*, 2:219–227, 1964. 10.1007/BF00528281.

[23] J. A. Pople. Electron interaction in unsaturated hydrocarbons. *Trans. Faraday Soc.*, 49:1375–1385, 1953.

[24] M. Chandross, S. Mazumdar, M. Liess, P. A. Lane, Z. V. Vardeny, M. Hamaguchi, and K. Yoshino. Optical absorption in the substituted phenylene-based conjugated polymers: Theory and experiment. *Phys. Rev. B*, 55:1486–1496, 1997.

[25] Robert J Bursill, Christopher Castleton, and William Barford. Optimal parametrisation of the pariser-parr-pople model for benzene and biphenyl. *Chemical Physics Letters*, 294(4-5):305 – 313, 1998.

[26] C. W. M. Castleton and W. Barford. Screening and the quantitative pi-model description of the optical spectra and polarizations of phenyl based oligomers. *The Journal of Chemical Physics*, 117(8):3570–3582, 2002.

[27] S. Ramasesha, I.D.L. Albert, and B. Sinha. Optical and magnetic properties of the exact ppp states of biphenyl. *Molecular Physics*, 72:537–547(11), 20 February 1991.

[28] Within EFT, the σ-electrons can be included explicitly at the expense of a larger basis, and this may be necessary in order to explain transport in some experiments.[29].

[29] Latha Venkataraman, Jennifer E. Klare, Iris W. Tam, Colin Nuckolls, Mark S. Hybertsen, and Michael L. Steigerwald. Single-molecule circuits with well-defined molecular conductance. *Nano Lett.*, 6(3):458–462, 2006.

[30] Hyunwook Song, Youngsang Kim, Yun Hee Jang, Heejun Jeong, Mark A. Reed, and Takhee Lee. Observation of molecular orbital gating. *NATURE*, 462(7276):1039–1043, 2009.

[31] Kristian S. Thygesen. Electron transport through an interacting region: The case of a nonorthogonal basis set. *Phys. Rev. B*, 73(3):035309, Jan 2006.

[32] K. R. Roby. On the justifiability of neglect of differential overlap molecular orbital methods. *Chemical Physics Letters*, 11(1):6 – 10, 1971.

[33] D. Baeriswyl, D. K. Campbell, and S. Mazumdar. In H. Kiess, editor, *Conjugated Conducting Polymers*. Springer-Verlag, Berlin, 1992.

[34] Jesus Hernandez-Trujillo, Miguel Costas, and Alberto Vela. Quadrupole interactions in pure non-dipolar fluorinated or methylated benzenes and their binary mixtures. *J. Chem. Soc., Faraday Trans.*, 89:2441–2443, 1993.

[35] J. O. Howell, J. M. Goncalves, C. Amatore, L. Klasinc, R. M. Wightman, and J. K. Kochi. Electron transfer from

aromatic hydrocarbons and their .pi.-complexes with metals. comparison of the standard oxidation potentials and vertical ionization potentials. *Journal of the American Chemical Society*, 106(14):3968–3976, 1984.

[36] Branka Kovac, Manijeh Mohraz, Edgar Heilbronner, Virgil Boekelheide, and Henning Hopf. Photoelectron spectra of the cyclophanes. *Journal of the American Chemical Society*, 102(13):4314–4324, 1980.

[37] Jeffrey A. Sell and Aron Kuppermann. Angular distributions in the photoelectron spectra of benzene and its monohalogenated derivatives. *Chemical Physics*, 33(3):367 – 378, 1978.

[38] Tsunetoshi Kobayoshi. A simple general tendency in photoelectron angular distributions of some monosubstituted benzenes. *Physics Letters A*, 69(2):105 – 108, 1978.

[39] W. Schmidt. Photoelectron spectra of polynuclear aromatics. v. correlations with ultraviolet absorption spectra in the catacondensed series. *The Journal of Chemical Physics*, 66(2):828–845, 1977.

[40] P. D. Burrow, J. A. Michejda, and K. D. Jordan. Electron transmission study of the temporary negative ion states of selected benzenoid and conjugated aromatic hydrocarbons. *The Journal of Chemical Physics*, 86(1):9–24, 1987.

[41] Atsunari Hiraya and Kosuke Shobatake. Direct absorption spectra of jet-cooled benzene in 130–260 nm. *The Journal of Chemical Physics*, 94(12):7700–7706, 1991.

[42] John P. Doering. Low-energy electron-impact study of the first, second, and third triplet states of benzene. *The Journal of Chemical Physics*, 51(7):2866–2870, 1969.

[43] Robert P. Frueholz, Wayne M. Flicker, Oren A. Mosher, and Aron Kuppermann. Electronic spectroscopy of benzene and the fluorobenzenes by variable angle electron impact. *The Journal of Chemical Physics*, 70(6):3057–3070, 1979.

[44] E. E. Koch and A. Otto. Optical absorption of benzene vapour for photon energies from 6 ev to 35 ev. *Chemical Physics Letters*, 12(3):476 – 480, 1972.

[45] Koichi Tamagawa, Takao Iijima, and Masao Kimura. Molecular structure of benzene. *Journal of Molecular Structure*, 30(2):243 – 253, 1976.

[46] Zsolt Ugray, Leon Lasdon, John Plummer, Fred Glover, James Kelly, and Rafael Marti. Scatter search and local nlp solvers: A multistart framework for global optimization. *INFORMS JOURNAL ON COMPUTING*, 19(3):328–340, 2007.

[47] T. O. Wehling, E. Şaşıoğlu, C. Friedrich, A. I. Lichtenstein, M. I. Katsnelson, and S. Blügel. Strength of effective coulomb interactions in graphene and graphite. *Phys. Rev. Lett.*, 106(23):236805, Jun 2011.

[48] Stefan Linden, Christian Enkrich, Martin Wegener, Jiangfeng Zhou, Thomas Koschny, and Costas M. Soukoulis. Magnetic response of metamaterials at 100 terahertz. *Science*, 306(5700):1351–1353, 2004.

[49] P. Baltzer, L. Karlsson, B. Wannberg, G. hrwall, D. M. P. Holland, M. A. MacDonald, M. A. Hayes, and W. von Niessen. An experimental and theoretical study of the valence shell photoelectron spectrum of the benzene molecule. *Chemical Physics*, 224(1):95 – 119, 1997.

[50] Kanhayalal Baheti, Jonathan A. Malen, Peter Doak, Pramod Reddy, Sung-Yeon Jang, T. Don Tilley, Arun Majumdar, and Rachel A. Segalman. Probing the chemistry of molecular heterojunctions using thermoelectricity. *Nano Letters*, 8(2):715–719, 2008. PMID: 18269258.

[51] Xiao, Xu, and Nongjian J. Tao. Measurement of single molecule conductance: benzenedithiol and benzenedimethanethiol. *Nano Letters*, 4(2):267–271, 2004.

[52] Renato B. Pontes, Frederico D. Novaes, Adalberto Fazzio, and Antnio J. R. da Silva. Adsorption of benzene-1,4-dithiol on the au(111) surface and its possible role in molecular conductance. *Journal of the American Chemical Society*, 128(28):8996–8997, 2006. PMID: 16834348.

[53] Sara Letardi and Fabrizio Cleri. Interaction of benzene thiol and thiolate with small gold clusters. *The Journal of Chemical Physics*, 120(21):10062–10068, 2004.

[54] Beatriz Cordero, Veronica Gomez, Ana E. Platero-Prats, Marc Reves, Jorge Echeverria, Eduard Cremades, Flavia Barragan, and Santiago Alvarez. Covalent radii revisited. *Dalton Trans.*, pages 2832–2838, 2008.

[55] B. N. J. Persson and E. Zaremba. Reference-plane position for the atom-surface van der waals interaction. *Phys. Rev. B*, 30(10):5669–5679, Nov 1984.

[56] D. E. Eastman. Photoelectric work functions of transition, rare-earth, and noble metals. *Phys. Rev. B*, 2(1):1–2, Jul 1970.

[57] K. Kaasbjerg and K. Flensberg. Image charge effects in single-molecule junctions: Breaking of symmetries and negative-differential resistance in a benzene single-electron transistor. *Phys. Rev. B*, 84:115457, Sep 2011.

[58] Su Ying Quek, Latha Venkataraman, Hyoung Joon Choi, Steven G. Louie, Mark S. Hybertsen, and J. B. Neaton. Aminegold linked single-molecule circuits: experiment and theory. *Nano Letters*, 7(11):3477–3482, 2007. PMID: 17900162.

[59] Su Ying Quek, Hyoung Joon Choi, Steven G. Louie, and J. B. Neaton. Length dependence of conductance in aromatic single-molecule junctions. *Nano Letters*, 9(11):3949–3953, 2009. PMID: 19751067.

[60] Sergey Kubatkin, Andrey Danilov, Mattias Hjort, Jerome Cornil, Jean-Luc Bredas, Nicolai Stuhr-Hansen, Per Hedegard, and Thomas Bjornholm. Single-electron transistor of a single organic molecule with access to several redox states. *Nature*, 425(6959):698–701, October 2003.

[61] M. Poot, E. Osorio, K. O'Neill, J. M. Thijssen, D. Vanmaekelbergh, C. A. van Walree, L. W. Jenneskens, and S. J. van der Zant. Temperature dependence of three-terminal molecular junctions with sulfur end-functionalized tercyclohexylidenes. *Nano Letters*, 6:1031–1035, 2006.

[62] A. Danilov, S. Kubatkin, S. Kafanov, P. Hedegard, N. Stuhr-Hansen, K. Moth-Poulsen, and T. Bjornholm. Electronic transport in single molecule junctions: Control of the molecule-electrode coupling through intramolecular tunneling barriers. *Nano Letters*, 8(1):1–5, 2008.

[63] M. Kiguchi, O. Tal, S. Wohlthat, F. Pauly, M. Krieger, D. Djukic, J. C. Cuevas, and J. M. van Ruitenbeek. Highly conductive molecular junctions based on direct binding of benzene to platinum electrodes. *Phys. Rev. Lett.*, 101(4):046801, Jul 2008.

[64] Svetla D. Chakarova-Käck, Elsebeth Schröder, Bengt I. Lundqvist, and David C. Langreth. Application of van der waals density functional to an extended system: Adsorption of benzene and naphthalene on graphite. *Phys. Rev. Lett.*, 96:146107, Apr 2006.

[65] Jess Wellendorff, Andre Kelkkanen, Jens Jorgen Mortensen, Bengt I. Lundqvist, and Thomas Bligaard. RPBE-vdW Description of Benzene Adsorption on Au(111). *TOPICS IN CATALYSIS*, 53(5-6):378–383, MAY 2010.

[66] Biswajit Santra, Angelos Michaelides, Martin Fuchs, Alexandre Tkatchenko, Claudia Filippi, and Matthias Scheffler. On the accuracy of density-functional theory exchange-correlation functionals for h bonds in small water clusters. ii. the water hexamer and van der waals interactions. *The Journal of Chemical Physics*, 129(19):194111, 2008.

[67] S. Arcidiacono, J. H. Walther, D. Poulikakos, D. Passerone, and P. Koumoutsakos. Solidification of gold nanoparticles in carbon nanotubes. *Phys. Rev. Lett.*, 94(10):105502, Mar 2005.

[68] Vincent P. A. Lonij, Catherine E. Klauss, William F. Holmgren, and Alexander D. Cronin. Can atomsurface potential measurements test atomic structure models? *The Journal of Physical Chemistry A*, 0(0), 0.

[69] Supriyo Datta. *Electronic Transport in Mesoscopic Systems*. Cambridge University Press, 1997.

[70] Justin P. Bergfield, Joshua D. Barr, and Charles A. Stafford. The number of transmission channels through a single-molecule junction. *ACS Nano*, 5(4):2707–2714, 2011.

[71] Justin P. Bergfield, Michelle A. Solis, and Charles A. Stafford. Giant thermoelectric effect from transmission supernodes. *ACS Nano*, 4(9):5314–5320, 2010.